1 **Characterization of Ozone Production in San Antonio, Texas Using Measurements of Total**

2 **Peroxy Radicals**

3 Daniel C. Anderson[1], Jessica Pavelec[1], Conner Daube[2], Scott C. Herndon[2], W. B. Knighton[3],

4 Brian M. Lerner[2], J. Robert Roscioli[2], Tara I. Yacovitch[2], Ezra C. Wood[1]

5 [1]Department of Chemistry, Drexel University, Philadelphia, PA, USA

6 [2]Aerodyne Research Inc., Billerica, MA, USA

7 [3]Department of Chemistry and Biochemistry, Montana State University, Bozeman, MT, USA

9 *Abstract*

10 Observations of total peroxy radical concentrations ($[XO_2] \equiv [RO_2] + [HO_2]$) made by the Ethane

11 CHemical AMPlifier (ECHAMP) and concomitant observations of additional trace gases made onboard

12 the Aerodyne Mobile Laboratory (AML) during May 2017 were used to characterize ozone production at

13 three sites in the San Antonio, Texas region. Median daytime $[O_3]$ was 48 ppbv at the site downwind of

14 central San Antonio. Higher concentrations of NO and XO_2 at the downwind site also led to median

15 daytime ozone production rates ($P(O_3)$) of 4.2 ppbv hr^{-1}, a factor of two higher than at the two upwind

16 sites. The 95th percentile of $P(O_3)$ at the upwind site was 15.1 ppbv hr^{-1}, significantly lower than values

17 observed in Houston. *In situ* observations, as well as satellite retrievals of HCHO and NO_2, suggest that

18 the region was predominantly NO_X-limited. Only approximately 20% of observations were in the VOC-

19 limited regime, predominantly before 11 am, when ozone production was low. Biogenic volatile organic

20 compounds (VOC) comprised 55% of total OH reactivity at the downwind site, with alkanes and non-

21 biogenic alkenes responsible for less than 10% of total OH reactivity in the afternoon, when ozone

22 production was highest. To control ozone formation rates at the three study sites effectively, policy

23 efforts should be directed at reducing NO_X emissions. Observations in the urban center of San Antonio

24 are needed to determine whether this policy is true for the entire region.

1.   Introduction

Tropospheric ozone (O_3) is a secondary air pollutant formed through a series of reactions involving volatile organic compounds (VOCs) and NO_X ($[NO_X] \equiv [NO] + [NO_2]$, where NO is nitric oxide and NO_2 is nitrogen dioxide). While tropospheric ozone exists naturally through stratospheric transport (Holton et al., 1995) and *in situ* tropospheric production, human activities have drastically perturbed these background values (Lamarque et al., 2005). Exposure to ozone adversely impacts human health, limiting lung and cardiac function, exacerbating chronic respiratory illnesses, and precipitating early mortality (Bell et al., 2006;Park et al., 2005;Jerrett et al., 2009;Silva et al., 2013). In response to these adverse impacts, in 2015 the United States Environmental Protection Agency (EPA) imposed an 8 hour ozone standard of 70 ppbv, lowering the exposure limit from the 75 ppbv standard set in 2008 (EPA, 2015). While ambient concentrations of the ozone precursor NO_X have declined significantly over much of the US (Choi and Souri, 2015;He et al., 2013;Duncan et al., 2016;Lamsal et al., 2015), reductions in ozone concentrations have been less dramatic. Background ozone concentrations have actually increased in some locations (Cooper et al., 2012;Choi and Souri, 2015); in other areas that have seen decreases in ambient ozone concentrations, such as Texas and the mid-Atlantic region, ozone still periodically exceeds the EPA standard (e.g. He et al., 2013).

Ozone production is generally classified as either NO_X- or VOC-limited (Kleinman, 1994;Thornton, 2002). Net formation of ozone occurs when NO is oxidized to NO_2 by reaction with the hydroperoxyl radical (HO_2) or an organic peroxy radical (RO_2). In the NO_X-limited regime, comparatively low concentrations of NO_X allow for the removal of RO_X radicals ($[RO_X] \equiv [OH] + [HO_2] + [RO_2]$, where OH is the hydroxyl radical) by self-reactions (e.g. Reactions R1 − R3). In the VOC-limited regime, RO_X radicals are removed from the atmosphere by reactions

49   with NO_X, producing less reactive compounds such as nitric acid (HNO_3) (Reactions R4 – R6).

50   In the NO_X-limited regime, reductions in NO_X lead to reductions in O_3; while in the VOC-

51   limited regime, reductions in NO_X without concomitant reductions in VOCs can actually increase

52   O_3 production. One prominent example of this is the weekday/weekend effect in the Southern

53   California Air Basin, where O_3 increases on weekends due to decreases in NO_X emissions from

54   heavy duty diesel trucks (Pollack et al., 2012). The effective implementation of ozone reduction

55   policies therefore requires a detailed understanding of the ozone production regime of the target

56   area.

$$HO_2 + OH \rightarrow H_2O + O_2 \qquad\qquad (R1)$$
$$HO_2 + HO_2 + M \rightarrow H_2O_2 + O_2 + M \qquad\qquad (R2)$$
$$HO_2 + RO_2 \rightarrow ROOH + O_2 \qquad\qquad (R3)$$
$$OH + NO_2 + M \rightarrow HNO_3 + M \qquad\qquad (R4)$$
$$NO + RO_2 + M \rightarrow RONO_2 + M \qquad\qquad (R5)$$
$$NO_2 + R(O)O_2 + M \rightarrow R(O)O_2NO_2 + M \qquad\qquad (R6)$$
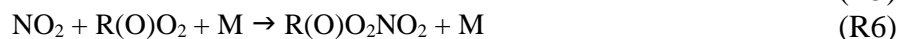
57

58   Texas is the second most populous state in the US. With multiple large urban centers

59   and a mixture of urban and industrial emissions from petrochemical processing facilities as well

60   as from natural gas and oil extraction, the state has complex pollution chemistry. This

61   combination of a large population and pollution makes understanding ozone production in this

62   region particularly important. Previous studies of ozone formation in Texas have focused

63   primarily on Houston and the surrounding region. Mazzuca et al. (2016) used *in situ*

64   observations of NO_X and O_3 from the DISCOVER-AQ campaign in summer 2013 along with

65   output from the CMAQ model to find significant diurnal variability in ozone production, with

66   higher ozone production rates ($P(O_3)$) in the morning and a transition from the VOC- to NO_X-

67   limited regime before afternoon. Similar results were found during the TEXAQS2000,

68   TRAMP2006, and SHARP 2009 campaigns (Mao et al., 2010;Ren et al., 2013). Multiple studies

69   have found that anthropogenic alkenes, particularly ethylene and propylene, are major

70   contributors to OH reactivity and therefore O_3 production (Mao et al., 2010;Kleinman et al.,

71   2002;Ryerson et al., 2003) in the region leading to $P(O_3)$ greater than 50 ppbv hr^{-1} (Mazzuca et

72   al., 2016). OH reactivity is defined as the sum of the products of the concentration of species X

73   and the reaction rate coefficient ($k_{X + OH}$) of X with OH (Eq. 1).

$$k_{OH} = \sum_i k_{(X+OH)}[X]_i \qquad (1)$$

74   There have been comparatively few field campaigns, however, to study San Antonio,

75   Texas, the seventh most populous city in the US. In July 2018, the EPA designated the San

76   Antonio region as being in marginal non-attainment with the new 70 ppbv standard, suggesting a

77   need to understand the O_3 formation chemistry in the region. In addition, San Antonio has a

78   significantly different emissions profile than Houston. For example, examination of long-term

79   VOC monitoring in Floresville, TX, a site immediately upwind of San Antonio, suggests that OH

80   reactivity is dominated by alkanes (Schade and Roest, 2016) in contrast with the dominance of

81   alkenes in Houston. Fig. 1 shows the trends in concentrations of ozone, NO_X, and O_X ($O_X \equiv O_3 +$

82   NO_2) at two Texas Commission on Environmental Quality (TCEQ) monitoring sites, with one

83   (Camp Bullis) located northwest of the urban center and the other (Pecan Valley) in the

84   downtown area (Fig. 2b). With the lowering of the 8-hour ozone standard from 75 ppbv (dashed

85   purple line) to 70 ppbv (solid purple line), the Camp Bullis site is much more likely to be in

86   exceedance, while the Pecan Valley site remains below both standards. Despite noticeable

87   decreases in maximum NO_X at both sites over the 14-year period shown here, there is little

88   noticeable trend in ozone. This is in agreement with Choi and Souri (2015), who found a $0.07 \times$

89   10^{15} $cm^{-2}yr^{-1}$ decrease in tropospheric column NO_2 over San Antonio between the years 2005

90   and 2014 while finding an increasing trend of 0.64 ppbv yr^{-1} in the minimum value of surface

91   ozone over the same period. Further study is needed in the San Antonio region to understand the

92   driving factors behind ozone production.

93   In this manuscript, we present results from the San Antonio Field Study (SAFS)

94   conducted in the San Antonio, Texas region in May 2017. We show observations of total peroxy

95   radical concentrations ($[XO_2] \equiv [RO_2] + [HO_2]$) from three sites in the San Antonio area,

96   characterizing the XO_2 distribution in the region. We use these XO_2 measurements, along with

97   observations of NO and other trace gas species, to quantify ozone production in regions up- and

98   downwind of the urban core. Though there have been many prior determinations of $P(O_3)$ using

99   measurements of a subset of peroxy radicals (*i.e.*, using laser-induced fluorescence

100   measurements of HO_2 and a fraction of RO_2) (e.g. Ren et al., 2013), this is one of the few

101   determinations of ozone production using the direct observation of total peroxy radicals

102   (Sommariva et al., 2011). Combined with quantification of the primary production of RO_X

103   radicals ($P(RO_X)$) and satellite retrievals of HCHO and NO_2, we determine the ozone production

104   regime in San Antonio. Finally, we explore the main contributors to OH reactivity in the region.

105   *2.   Methodology*

106   *2.1   Campaign Description*

107   The SAFS campaign was conducted from 11 to 31 May 2017 at several sites in the

108   greater San Antonio region. We describe measurements made on the Aerodyne Mobile

109   Laboratory (AML) at three sites: the University of Texas San Antonio (UTSA) from 11 to 16

110   May and from 27 to 31 May, Floresville, Texas from 16 to 21 May, and Lake Corpus Christi

111   (Corpus) from 21 to 26 May. The sites were chosen to determine the impact of various emission

112   sources on ozone formation affecting San Antonio. During May in southeastern Texas, the

113   prevailing wind direction is southeasterly, coming off the Gulf of Mexico. UTSA is located

114   northwest (*i.e.* downwind) of downtown San Antonio (Fig. 2a) while the Floresville and Corpus

115   sites were both located upwind of the city. This allows for the determination of background

116   values of compounds through observation at the Floresville and Corpus sites, while observations

117   at UTSA are more representative of air photochemically processed with urban emissions. We

118   define background here as values upwind of the UTSA site. The AML was situated at all sites to

119   minimize influence from local emissions. At UTSA, the AML was located in a mostly vacant

120   parking lot about 1 km south of the nearest major roadway. In Floresville and Corpus, there

121   were no nearby major roadways, local traffic was at a minimum, and influence from local point

122   and mobile sources was limited. Potential influences from transient local sources (e.g. lawn

123   mowers and jet skis) were removed in the same manner as interference from the generator

124   emissions described below.

125   The AML is outfitted to measure a suite of gas- and particle-phase atmospheric species

126   (Herndon et al., 2005). All instrument inlets were mounted approximately 15 m above ground

127   level on a retractable tower located near the AML. At both the Floresville and UTSA sites, the

128   AML was powered through connection to the local electric utility while at Corpus a diesel

129   generator was used. Although the generator was situated downwind of the instrument inlets,

130   some stagnation and recirculation did occur, allowing for occasional sampling of generator

131   exhaust. Air parcels affected by the generator exhaust were removed through analysis of CO

132   observations. A filter for generator-influenced air was created by determining the minimum CO

133   value over a 100 s period every 5 minutes. Any air parcel with a CO mixing ratio 10 ppbv

134   higher than this minimum was assumed to be impacted by a local transient source, including the

135   generator.

136   Trace gases measured during SAFS and used in this study are summarized here. Unless

137   otherwise indicated, data used in this study were reported as 1-minute averages and then

138   averaged to the 2-minute Ethane CHemical AMPlifier (ECHAMP) time base, described in the

139   following section. NO_2 was measured at 1 Hz via Cavity Attenuated Phase Shift (CAPS)

140   spectroscopy (Kebabian et al., 2005;Kebabian et al., 2008). Nitric oxide (NO) was measured at

141   0.1 Hz through the same inlet as NO_2 and O_3 using a Thermo Fisher 42i-TL chemiluminescence

142   analyzer, while O_3 was measured with a 2B-Tech model 205 ultraviolet (UV) absorption

143   instrument. Uncertainties (2σ) of the NO, NO_2, and O_3 observations on the ECHAMP

144   measurement time scale are below 5%. The above instruments were zeroed every 15 minutes

145   with humidity-matched zero air. The zero air was generated by passing ambient air through an

146   Aadco ZA30 Catalyst system for VOC removal and through Purafill Chemisorbant Media, a

147   potassium permanganate based scrubber, for NOx removal.

148   Quantum Cascade – Tunable Infrared Laser Direct Absorption Spectrometers (QC-

149   TILDAS) from Aerodyne Research Inc. (ARI) were used to measure CO and H_2O (2200 cm^{-1};

150   measurement wave number), HCHO (1765 cm^{-1}), CH_4 and C_2H_6 (2990 cm^{-1}), H_2O_2 (1277

151   cm^{-1}), and C_3H_8 (2965 cm^{-1}) (McManus et al., 2015). A Proton Transfer Reaction – High

152   Resolution – Time of Flight (PTR-HR-ToF) mass spectrometer was used to measure isoprene,

153   acetaldehyde, acetone, benzene, methanol, the sum of monoterpenes, the sum of methyl vinyl

154   ketone (MVK) and methacrolein, and toluene. Typical measurement uncertainties were on the

155   order of 25%. Finally, a prototype of a commercially-available gas chromatograph from ARI

156   with electron-impact time-of-flight mass spectrometer (GC-EI-ToF-MS) was used to measure a

157   suite of VOCs, including isoprene, 1,2,3-trimethylbenzene, ethyl benzene, cyclohexane, *n*-

158   heptane, *n*-hexane, *n*-octane, *n*-pentane, *o*-xylene, and the sum of *m*- and *p*- xylenes. The GC

159   sampled with a multi-component adsorbent trap (Pollmann et al., 2006) for a 5 minute

160   integration period every 20 minutes. GC observations are unavailable for 20-30 May. While

161   toluene and *m-* and *p-* xylene measurement uncertainty was on the order of 20%, typical

162   measurement uncertainties of other observed species, except isoprene, were on the order of 10%.

163   While there were two independent observations of isoprene, there were limitations with

164   both methods. It was determined that the actual isoprene concentration in the calibration

165   standard used in the field for the PTR had degraded over time, resulting in erroneously high

166   isoprene values. On the other hand, the GC was not calibrated for isoprene during the campaign

167   and observations are only available for half the time. As a result, we use the PTR isoprene from

168   the entire campaign scaled to the GC values, using a GC isoprene sensitivity determined after the

169   campaign. This method results in an estimated isoprene uncertainty of ≈30% (1σ). See the SI

170   for more information.

171   Temperature, wind speed, and wind direction were measured at the top of the inlet tower

172   with a 3D RMYoung (Model 81000RE) sonic anemometer. Atmospheric pressure observations

173   used in this study were taken from the National Weather Service observations at the San Antonio

174   International Airport for the UTSA and Floresville sites and from the Corpus Christi

175   International Airport for the Corpus site. NO_2 photolysis frequencies (J_{NO2}) were measured via a

176   filter radiometer (MetCon, GmbH) located on top of the AML (Shetter et al., 2003;Stark et al.,

177   2007).

178   *2.2   ECHAMP*

179   Total peroxy radical concentrations ($[XO_2]$) were measured via chemical amplification by

180   the ECHAMP instrument. A complete instrument description can be found in Wood et al.

181   (2017), and only the most relevant details are summarized here, including a new sampling

182   system that includes an integrated, remotely-controlled RO_X calibration source. Briefly,

183   ECHAMP measures total XO_2 concentration at a two-minute resolution by reacting peroxy

184   radicals with excess NO and ethane (C_2H_6). Through a series of chain reactions, each XO_2

185   radical produces approximately 20 NO_2 molecules (depending on the relative humidity (RH)),

186   which are then measured with a commercially available NO_2 monitor. Because this NO_2 monitor

187   also measures ambient O_3 and NO_2 (O_X), a second channel and dedicated NO_2 monitor are used

188   to only measure the sum of $[O_3]$ and $[NO_2]$. The difference between the two channels, divided

189   by the "amplification factor" of ~20, yields the XO_2 concentration.

190   The inlet box is a 39 cm × 44 cm × 16 cm fiberglass, rainproof electrical enclosure. The

191   box was mounted at the top of the sampling tower and connected to the rest of the instrument via

192   a bundle of tubes and electrical cables. Ambient air was sampled at a flow rate of 6.5 LPM

193   through 76 mm of 3.6 mm inner diameter (ID) glass into the inlet box (see Fig. S1 for a

194   schematic of the plumbing). The glass was internally coated with halocarbon wax to minimize

195   wall losses of XO_2. The flow was sub-sampled into two, 1.9 cm^3 reaction chambers at a flow

196   rate of 1.1 LPM each. Temperature and RH of the remaining 4.5 LPM of sampled air were

197   measured with a Vaisala probe (Model HMP60). Laboratory tests over a range of flow rates and

198   RH have demonstrated sampling losses of HO_2 of less than 3% and negligible losses of CH_3O_2

199   (Kundu et al., 2019).

200   Reaction chambers cycled every minute between an amplification mode and a

201   background mode, for a total cycle time of 2 minutes. In both modes, 25 sccm of 39.3 ppmv NO

202   in N_2 (Praxair) was added at the beginning of the reaction chamber, resulting in a final NO

203   mixing ratio of 0.90 ppmv. In amplification mode, 35 sccm of a 42.2% ethane mixture in N_2

204   (Praxair) was also added to the sampled air at the beginning of the reaction chamber. The radical

205   propagation scheme shown in reactions R7 – R13, in which Reactions (R9) – (R13) repeat

206   numerous times, results in formation of NO_2. The number of NO_2 molecules formed per XO_2

207   molecule sampled is known as the amplification factor (F) and varies with RH. During SAFS, F

208   was 23 for dry air and decreased to 12 at 58% RH. The two calibration methods used to

209   determine F are described below and more fully in the SI. At 15.2 cm downstream of the

210   NO/C_2H_6 injection point, 35 sccm of N_2 was added to the flow. In the background chamber, the

211   N_2 and C_2H_6 flows were switched (N_2 was added upstream, and C_2H_6 was added downstream),

212   allowing XO_2 radicals to react with NO to form HONO or alkyl nitrates before 35 sccm of the

213   42.2% ethane mixture was added at the end of the reaction chamber. The resultant NO_2 from

214   each chamber was then measured with separate, dedicated CAPS instruments. Total XO_2 was

215   then determined by the difference between the two NO_2 measurements divided by F.

$$RO_2 + NO \rightarrow RO + NO_2 \qquad\qquad (R7)$$
$$RO \rightarrow HO_2 + products \qquad\qquad (R8)$$
$$HO_2 + NO \rightarrow OH + NO_2 \qquad\qquad (R9)$$
$$OH + C_2H_6 \rightarrow H_2O + C_2H_5 \qquad\qquad (R10)$$
$$C_2H_5 + O_2 + M \rightarrow C_2H_5O_2 + M \qquad\qquad (R11)$$
$$C_2H_5O_2 + NO \rightarrow C_2H_5O + NO_2 \qquad\qquad (R12)$$
$$C_2H_5O + O_2 \rightarrow CH_3CHO + HO_2 \qquad\qquad (R13)$$
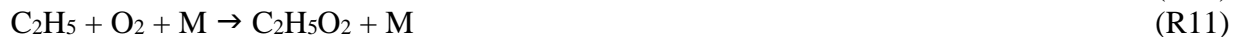
216

217   The CAPS instruments were calibrated for NO_2 before, after, and once during

218   deployment via quantitative reaction of known concentrations of O_3 generated with a 2B

219   Technologies ozone generator (Model 306) with excess NO. This ozone source agreed within

220   1% with a separate Thermo ozone generation source (Model 49C). All NO_2 calibrations agreed

221   within 5%. The amplification factor (F) was determined by producing known amounts of peroxy

222   radicals by two calibration methods: photolysis of H_2O and of CH_3I. Both methods are described

223   in more detail in the SI. Briefly, the H_2O photolysis method is similar to that used by most HO_X

224   instruments, in which H_2O was photolyzed at a wavelength of 184.9 nm to form an equimolar

225 mixture of OH and HO_2 (Mihele and Hastie, 2000;Faloona et al., 2004). This mixture was then

226 reacted with H_2 to convert the OH into HO_2. Radical concentrations were quantified using the

227 relevant spectroscopic parameters and the measured H_2O and O_3 concentrations in the calibration

228 gas.

229   The second calibration method was based on 254 nm photolysis of CH_3I in humidified

230 air, producing the CH_3O_2 radical. The radical concentration is quantified by reaction of the

231 CH_3O_2 with NO in the absence of C_2H_6, producing 1.86 NO_2 molecules per CH_3O_2. The H_2O

232 photolysis method was performed 6 times, while the CH_3I method was performed once during

233 the field campaign, on 31 May. Both methods were repeated twice in the laboratory after the

234 campaign. Observations from ECHAMP agreed within 12% with the H_2O photolysis calibration

235 source operated by Indiana University during a comparison study in 2015 (Kundu et al., 2019).

236 For the XO_2 observations described in this paper, we use the CH_3I calibration. While both

237 methods agree within uncertainty, the H_2O photolysis method was only conducted for RH values

238 of less than approximately 20%, much lower than typical ambient RH. See the SI for further

239 information.

240   The total 2σ accuracy for XO_2 during SAFS was approximately 25%. Calibrations were

241 not performed at RH values greater than 71%. Therefore, we omit all observations with a sample

242 RH greater than 71%. Approximately 85% of these high RH points were observed at nighttime,

243 so we only consider daytime data (7:00 – 20:00 local time) unless otherwise indicated.

244 *2.3   Calculation of P(O₃) and P(ROₓ)*

245   We use measurements of XO_2 and NO to calculate the gross rate of ozone production

246 $P(O_3)$ using Eq. (2), in which k_{NO+HO2} is the reaction constant for the reaction of NO with HO_2

247 and k_i is the reaction constant for NO with an organic peroxy radical $[RO_2]_i$. We note that this is

248 more accurately described as the rate of odd oxygen (O_X) production. Because ECHAMP only

249 measures the sum of peroxy radicals and not their speciation, we assume a simplified form of

250 this relationship (Eq. 3), where k_{eff} is an effective rate constant taken as that of k_{NO+HO2}. Box

251 modeling results for this site, which will be discussed more fully in a forthcoming paper, show

252 the dominant XO_2 species are HO_2, CH_3O_2, and isoprene RO_2. At 298 K, k_{NO+HO2} is within 10%

253 of the k values for the reaction of NO with CH_3O_2 and isoprene RO_2 (Orlando and Tyndall,

254 2012), supporting our choice of k_{eff}. Further, while the reaction of NO with acetyl peroxy

255 radicals is approximately 2.5 times faster than with other peroxy radicals at 298K, box modeling

256 results suggest that these radicals comprise only $5 - 10\%$ of total XO_2, resulting in an average

257 difference in P(O_3) of 15% from the k_{NO+HO2} value used here. This uncertainty is comparable to

258 the total uncertainty of the k_{NO+HO2} rate constant, estimated as 15% (Sanders et al., 2011). As will

259 be shown in Section 3.2, our conclusions are insensitive to the value of k_{eff} chosen. Uncertainty

260 in gross P(O_3) results from uncertainty in the NO and XO_2 measurements, 5% and 25%,

261 respectively, and k_{eff}, whose uncertainty we estimate at 23%, determined by adding the

262 uncertainty in the k_{NO+HO2} rate constant and the uncertainty in the choice of k_{eff} in quadrature.

263 This results in a total P(O_3) uncertainty of 34%.

$$P(O_3)_{Gross} = k_{NO+HO2}[NO][HO_2] + [NO]\sum_i k_i[RO_2]_i \tag{2}$$

$$P(O_3)_{Gross.} = k_{eff}[NO][XO_2] \tag{3}$$

$$L(O_3) = \left(\frac{k_{O1D+H2O}[H_2O]}{k_{O1D+H2O}[H_2O] + k_{O1D+N2}[N_2] + k_{O1D+O2}[O_2]} J_{O1D} + k_{OH+O3}[OH] \right. \tag{4}$$
$$\left. + k_{HO2+O3}[HO_2] + \sum_i k_{alkene-i}[alkene_i] \right)[O_3]$$
$$+ k_{OH+NO2}[OH][NO_2][M]$$

264

265   The net formation rate of O_3 is equal to $P(O_3)_{Gross} - L(O_3)$. In order to tie $P(O_3)$

266   completely to observations, we report only gross $P(O_3)$, not net $P(O_3)$. That is, we only calculate

267   the production term (Eq. 2) and not the loss term (Eq. 4) for net ozone production. Calculation

268   of the loss term requires knowledge of the concentration of OH and alkenes as well as the

269   fraction of total XO_2 comprised of HO_2, none of which were measured during SAFS. Alkene

270   concentrations, except for isoprene and monoterpenes, were not measured during SAFS.

271   Estimating the alkene loss term using concentrations from nearby TCEQ monitoring sites,

272   suggests that O_3 loss due to this pathway is negligible for the data analyzed here, and we omit

273   this from our calculation of ozone loss. To estimate OH and the fraction of XO_2 comprised of

274   HO_2 and to determine whether analyzing only gross $P(O_3)$ affects our conclusions, we used the

275   Framework for 0-Dimensional Atmospheric Modeling (F0AM) box model (Wolfe et al., 2016b)

276   to calculate OH and the fraction of RO_2 comprised of HO_2. A description of the model setup can

277   be found in the SI. For data points that were not modeled due to missing model constraints,

278   these values were estimated from interpolation of modeled values, if observations were made

279   within two hours of a modeled data point, or from site-specific mean daily profiles if no modeled

280   points were available. Using these modeled-derived values for OH and the HO_2 fraction, median

281    $L(O_3)$ for daytime observations at all sites were determined to be 0.90 ppbv/hr, which is 16% of

282   the gross production rate.

283   We use Eq. (5) to calculate the primary RO_X production rate. Here, $P(RO_X)$ is the RO_X

284   production rate, J indicates photolysis rate, and $k_{O1D+H2O}$, k_{O1D+O2}, and k_{O1D+N2} are the reaction

285   rate constants for the reaction of O_{1D} with the indicated species. The Tropospheric Ultraviolet

286   and Visible (TUV) model was used to calculate photolysis rate constants (J values), which were

287   then scaled to the measured J_{NO2}. HONO was not measured during SAFS. We estimate HONO

288   concentrations assuming an upper limit to the [HONO]/[NOx] ratio of 0.04 as described in Lee et

289   al. (2013). This is an upper bound on the HONO concentration and thus on HONO contribution

290   to P(ROx). Alkene concentrations were estimated from nearby TCEQ monitoring sites, as

291   described in Sect. 3.3. Alkene ozonolysis was calculated to have a negligible impact on P(ROx)

292   and is omitted from the analysis.

$$P(RO_X) = 2J_{O1D}[O_3]\frac{k_{O1D+H2O}[H_2O]}{k_{O1D+H2O}[H_2O]+k_{O1D+N2}[N_2]+k_{O1D+O2}[O_2]} + 2J_{HCHO}[HCHO] +$$

$$2J_{CH3CHO}[CH_3CHO] + 2J_{Acetone}[CH_3COCH_3] + 2J_{H2O2}[H_2O_2] + J_{HONO}[HONO]$$

(5)

293   Total P(ROx) peaks at midday at about 0.65 pptv s^{-1} on average and is dominated by the ozone

294   and HCHO terms, terms 1 and 2 from Eq. (5), respectively, with contributions from the other

295   observed species totaling less than 5% on average. Contributions from HONO were generally

296   less than 0.1 pptv s^{-1}, even assuming the upper bound in the HONO to NOx ratio used here.

297   *2.4*   *Satellite Data*

298   We use observations of NO_2 and HCHO from the Ozone Monitoring Instrument (OMI) to

299   provide a remotely-sensed estimate of the surface ozone production regime in San Antonio

300   (Duncan et al., 2010;Ring et al., 2018). OMI has a local overpass time of about 13:30 and

301   provides daily, global coverage. The instrument measures backscattered solar radiation in the

302   UV/visible region, allowing for differential optical absorption spectroscopy (DOAS) type

303   retrievals of multiple species, including NO_2 and HCHO.

304   For NO_2, we use the NASA Goddard Space Flight Center (GSFC) version 3 level 2

305   tropospheric column product (Bucsela et al., 2013;Krotkov et al., 2017) gridded to 0.25º latitude

306    $\times$ 0.25º longitude resolution. For HCHO, we use the version 3 level 2 reference sector corrected

307   swath product from the Harvard-Smithsonian Astrophysical Observatory (SAO) retrieval

308   (González Abad et al., 2015) also on a 0.25º latitude $\times$ 0.25º longitude grid. For both OMI

309 products, we use only pixels that satisfy quality and row anomaly flags, have a cloud fraction

310 less than 30%, and a solar zenith angle less than 70°. Additionally, data from the two outer most

311 pixels are removed due to their large footprint (28km × 150km) compared to the nadir view.

312   We analyze the HCHO to NO_2 ratio using OMI data from May to July 2017. While

313 SAFS lasted only one month, missing data due to cloud cover, the row anomaly, and other

314 factors necessitate a longer time period for data averaging. To calculate the ratio of HCHO to

315 NO_2, we first calculate the standard deviations (σ) of the HCHO and NO_2 data at each grid point.

316 When calculating the ratio, we only include days within 2σ of the average HCHO and NO_2

317 observations and only include grid boxes that have at least 10 days with coincident observations

318 of both species.

319 *3. Results*

320 *3.1 Distribution of Ozone and its precursors*

321   The highest ozone mixing ratios observed at UTSA were on 14 and 15 May, reaching a

322 maximum near 80 ppbv, while daytime values typically varied between 40 and 60 ppbv during

323 the remainder of the campaign (Fig. 3). Median daytime [O_3] at all three measurement sites was

324 37 ppbv (Fig. 4a). Median ozone was 18 ppbv higher at UTSA than at the background site in

325 Floresville. Although the highest ozone values were seen at UTSA, there was significant overlap

326 in the ozone distribution between the UTSA and Corpus sites. Consistent with the higher O_3

327 abundance, concentrations of the O_3 precursors isoprene, NO, and XO_2 were also highest at the

328 UTSA site. Median isoprene concentrations, one of the largest contributors to OH reactivity as

329 will be shown later, was almost two orders of magnitude larger at UTSA (1.2 ppbv) than at the

330 other sites (0.05 and 0.03 ppbv at Floresville and Corpus, respectively). While the difference in

331 median [NO] at the sites was not as extreme, a much larger range was seen at UTSA, where the

332   95th percentile of observations was above 2 ppbv. Similar results are seen for the [XO_2]

333   distribution (Fig. 4c), with the highest XO_2 mixing ratios (90 pptv) coinciding with the maximum

334   O_3. Median [XO_2] was approximately 1.5 times higher at the UTSA site (37 pptv) than at

335   Floresville (26 pptv) and Corpus (25 pptv).

336   XO_2 concentrations showed a distinct diurnal profile (Fig. 5). Overnight values were

337   approximately constant with a median of around 10 pptv, until a small decline after 3:00. A

338   steady increase in [XO_2] began at 9:00, with a peak of 50 pptv at 15:00 and then a decline to the

339   overnight value by 20:00. The shape of this profile is in agreement with other observations of

340   peroxy radicals from a variety of chemical environments (Sanchez et al., 2016;Mao et al.,

341   2010;Whalley et al., 2018). Noise in the nighttime data is a result of higher RH and thus

342   degraded precision of the ECHAMP measurement technique and is not an indication of

343   significant nighttime variability. Even though we have filtered for data points with RH greater

344   than 71% as discussed in Sect. 2.2, nighttime RH is higher than daytime values, on average,

345   decreasing measurement precision. Daytime variability resulted from changes in insolation and

346   biogenic VOC concentrations. The days that showed little or no diurnal profile at UTSA and

347   Corpus were overcast, as evidenced by low J_{NO2} (Fig. 3). Concentrations of isoprene and the sum

348   of methyl vinyl ketone (MVK) and methacrolein, both isoprene degradation products, were at a

349   maximum when [XO_2] peaked at 90 pptv.

350   The higher O_3 concentrations at UTSA are consistent with its location downwind of the

351   urban core of San Antonio. Figure S2 shows wind roses colored by ozone and the ozone

352   precursors described above. The wind direction while at UTSA was predominantly

353   southeasterly, in agreement with the climatological average for the region. The highest ozone

354   mixing ratios, as well as the highest XO_2 and isoprene, were seen when air parcels originated

355 from this direction, travelling over the city. The highest [NO] (greater than 2.2 ppbv), however,

356 was seen with northerly and northeasterly winds. This is likely because of the proximity of a

357 major highway north of the UTSA site, which would provide a source of recently-emitted, less

358 processed emissions than in air parcels that travelled from downtown San Antonio. The CO

359 distribution by wind direction (not shown) is consistent with this explanation.

360 *3.2 Ozone production*

361 The highest $P(O_3)$ values (and highest [NO] and [XO_2]) were observed at UTSA. Median

362 $P(O_3)$ between 7:00 and 20:00 at UTSA was 4.1 ppbv hr^{-1}, compared to just over 1 ppbv hr^{-1} at

363 both Floresville and Corpus. The 95th percentile, 12.6 ppbv hr^{-1}, is significantly lower than rates

364 found in Houston, which frequently topped 40 ppbv hr^{-1} (Mazzuca et al., 2016;Mao et al., 2010).

365 As with [O_3] and [XO_2], the highest $P(O_3)$ rates occurred when winds travelled over downtown

366 San Antonio.

367 Figure 6a shows the variation in $P(O_3)$ with [NO], where the data points have been

368 colored by $P(RO_X)$ for all observations taken during SAFS. The relationship for the subset of

369 observations exclusively at UTSA is essentially identical. In general, $P(O_3)$ increases with

370 [NO], although a wide range of $P(O_3)$ exists for a given value of NO. For a constant value of

371 [NO], $P(O_3)$ is consistently higher at higher $P(RO_X)$. Figure 6b shows the same data as panel 6a

372 but binned both by NO mixing ratio and $P(RO_X)$. All $P(O_3)$ observations have been separated

373 into NO bins with an equal number of observations, as well as into two bins of $P(RO_X)<0.2$ and

374 $P(RO_X)>0.4$. The values of $P(RO_X)$ were chosen to represent the low and high ranges of $P(RO_X)$

375 observed during SAFS. The conclusions drawn from the results are insensitive to the values

376 chosen for these bins.

377 Figure 6b demonstrates that the majority of observations made during SAFS were in the

378 NO_X-limited regime. For the high $P(RO_X)$ observations, there is a steady increase in $P(O_3)$ up to

379   the 500 pptv NO bin. Above this point, $P(O_3)$ potentially plateaus, but there were insufficient

380   observations at higher NO to determine the location of the turnover point in ozone production.

381   Because the majority of NO observations at UTSA were less than 500 pptv, we conclude that the

382   site is predominantly NO_X-limited. Further observations at higher NO mixing ratios are required

383   to determine the turnover point for ozone production in this region. The true turnover

384   concentration for NO cannot be easily inferred by inspection of a graph of $P(O_3)$ versus [NO],

385   however, because VOC concentrations are not constant for all points. To see if there is any

386   variation in this relationship with VOCs, we further separate the high $P(RO_X)$ data by their VOC

387   reactivity (Fig. S3). VOC reactivity (VOCR) was calculated in the same manner as OH

388   reactivity, described in section 3.3, but including only OH reactive VOCs. In addition, VOCs

389   exclusively observed by the GC instrument were not included in the calculation as they were

390   only available until 19 May. For data points with GC observations available, VOC reactivity

391   increased by only 2% in the afternoon and 12% in the morning on average when including the

392   GC observations, suggesting that this omission does not significantly affect the results.   Data

393   were then separated into low (VOCR < 3 s^{-1}), medium (3 s$^{-1} <$ VOCR < 6 s^{-1}), and high (6 s^{-1} $<$

394   VOCR < 9 s^{-1}) VOC reactivity bins. For the high $P(RO_X)$ case, the relationship is similar for all

395   VOC reactivities, showing a general increase in $P(O_3)$ with NO, further suggesting the majority

396   of observations were NO_X-limited for high $P(RO_X)$. We note that for a constant $P(RO_X)$ value,

397   theoretically $P(O_3)$ is expected to increase with [NO] at approximately the same rate until the

398   turn-over point with little sensitivity to the VOC reactivity. The 5th and 95th percentiles of

399    $P(RO_X)$ for the high $P(RO_X)$ are 0.42 and 0.92 pptv s^{-1}, more than a factor of two different.   This

400   suggests that the differences in the rate of change of $P(O_3)$ with NO for the different VOC

401   reactivities likely results from the wide range of $P(RO_X)$ values analyzed.

402   When looking at all points for the low $P(RO_X)$ case (Fig. 6b), there is a small peak in

403    $P(O_3)$ at 200 pptv NO, suggesting that in a low $P(RO_X)$ environment, UTSA can be VOC-limited

404   at higher NO mixing ratios. Separating these data points by VOC reactivity, shows more clearly

405   the transition between the NO_X- and VOC-limited regimes. For the medium case, $P(O_3)$ first

406   increases with [NO], peaks at 5 ppbv hr^{-1} at approximately 200 pptv [NO], and then declines to 2

407   ppbv hr^{-1} at 400 pptv [NO]. This peak and decline suggests that, for $P(RO_X) < 0.2$ pptv/s, VOC

408   reactivities < 6 s^{-1}, and NO > 200 pptv, the region is VOC-limited. For NO > 400 pptv, there is a

409   slight increase in $P(O_3)$ with [NO], although the spread of data for a given [NO], also increases.

410   For the low VOC reactivity scenario, the range of $P(O_3)$ for a given [NO] is also large compared

411   to the mean $P(O_3)$, making it difficult to determine whether these points obey a similar

412   relationship. As with the high $P(RO_X)$ scenario, each bin has a wide range of $P(RO_X)$ and VOC

413   reactivities, which could lead to the large spread in data, suggesting the need for further

414   observations. Separating the results by location yields the same results, although VOC reactivity

415   at Floresville and Corpus were almost always below 3 s^{-1} due to the lower isoprene concentration

416   at these sites in comparison to UTSA.

417   Ozone production rates in VOC-limited regime are typically below 5 ppbv hr^{-1} and

418   constitute only 20% of the observations examined here, suggesting that the all three SAFS sites

419   are predominantly NO_X-limited. The majority of the VOC-limited points here (75%) occur

420   before 11 EDT, when NO concentrations are higher and isoprene emissions and VOC reactivity

421   are low. This is in agreement with the L_n/Q diurnal profile discussed below. For the NO_X-

422   limited points, increases in VOC concentrations are expected to have a small impact on $P(O_3)$;

423   for the VOC-limited points, increases in VOCs will lead to increased $P(O_3)$.

424     Finally, the results presented here are insensitive to the value of k_{eff} chosen. Figure S4

425  shows the relationship between $P(O_3)$ and NO for four different values of k_{eff}: k_{NO+HO2} (the k_{eff}

426  used in this analysis), $k_{NO+CH3O2}$, $k_{NO+IsopreneRO2}$, and assuming $k_{no+acetyl\ peroxy}$ for 10% of the value

427  and k_{NO+HO2} for the remainder. While the magnitude of $P(O_3)$ does change with k_{eff}, the overall

428  relationship is the same. As mentioned previously, the uncertainty in k_{NO+HO2} is larger than the

429  uncertainty induced by the choice of k_{eff}. Additional analysis further suggests that the majority

430  of the observations during SAFS were in the NO_X-limited regime.

431     These results are consistent with the diurnal profile of the ozone production regime as

432  determined by the separate "L_N/Q" metric, which is the ratio of the RO_X loss rate due to reactions

433  with NO_X (e.g., R3) to the total RO_X loss rate (Q) (Kleinman, 2005). In general, when more than

434  half of the RO_X loss is due to reaction with NO_X species ($L_N/Q > 0.5$) then $P(O_3)$ is VOC-

435  limited, whereas when the majority of RO_X loss is due to peroxy radical self-reactions ($L_N/Q <$

436  0.5) $P(O_3)$ is NO_X-limited. The Framework for 0-Dimensional Atmospheric Modeling (F0AM)

437  photochemical box model (Wolfe et al., 2016b), constrained to observations, was used to model

438  the parameters needed to calculate L_N/Q at the SAFS sites. A full description of the model setup

439  is in the SI. Using the box model results and the method described in Kleinman (2005), we

440  calculated L_N/Q for all box-modeled observations at UTSA (Fig. 7). A clear diurnal pattern is

441  evident with an early morning maximum and then a quick decline to $L_N/Q < 0.5$ at 9:00, after

442  which the ratio remains below 0.1 for the remainder of the day. At 18:00, however, the ratio

443  does begin to increase, though remaining well in the NO_X-limited space. While L_N/Q is highest

444  in the morning, $P(O_3)$ is at a minimum during this time period, suggesting that there is little O_3

445  production when $P(O_3)$ is VOC-limited. Furthermore, time periods where ozone was found

446  under VOC-limited conditions were likely confined to a relatively small volume of air in the

447 shallow, morning boundary layer. This transition from VOC- to NO_X-limited between morning

448 and afternoon is consistent with other locations (Mazzuca et al., 2016;Mao et al., 2010;Ren et al.,

449 2013) and the high NO concentrations that build up in the morning from local traffic and a low

450 boundary layer.

451   Finally, remotely sensed observations of NO_2 and HCHO from the OMI satellite

452 corroborate the conclusion that ozone production in San Antonio is NO_X-limited. The ratio of

453 column HCHO to tropospheric column NO_2 has been used as an indicator of the ozone

454 production regime in multiple regions (Duncan et al., 2010;Ring et al., 2018). According to

455 Duncan et al. (2010), a region is considered NO_X-limited when this ratio is greater than 2, VOC-

456 limited for values less than 1, and in a transition region for ratios between 1 and 2. Other studies

457 dispute these ranges, claiming that, in Houston, the NO_X-limited regime only begins for a ratio

458 greater than 5 (Schroeder et al., 2017). Figure 2 shows the ratio averaged over the months May –

459 July 2017 over Texas. In agreement with the *in situ* observations and the above analysis, the

460 satellite data places all three locations in the NO_X-limited regime with ratios much greater than 5.

461 Though they provide much higher spatial coverage, polar orbiting satellite observations are

462 limited in that they provide coverage once daily and that data must be averaged over a long

463 period to gain meaningful statistics. Likewise, because of the satellite footprint, any small

464 regions in urban centers that may be VOC-limited might not be evident here because of spatial

465 averaging. Nevertheless, the combination of satellite and *in situ* observations clearly

466 demonstrates that, at least at the three measurement sites, ozone production was NO_X-limited.

467 *3.3 OH Reactivity*

468   In contrast with Houston, the OH reactivity, and thus ozone production, at the UTSA

469 measurement site was driven by biogenic species, particularly isoprene. Figure 8 shows the OH

470 reactivity for the UTSA and Floresville sites. Observations after 19 May were excluded because

471   of the lack of GC observations. Concentrations of all observed OH reactive species were used to

472   calculate the total OH reactivity. These values were then divided into 5 groups: biogenics

473   (isoprene, MVK, methacrolein, and α-pinene), carbonyls (HCHO and acetaldehyde), alkanes

474   (ethane, propane, cyclohexane, octane, heptane, hexane, and pentane), NO_X, CO, CH_4, O_3, and

475   other (benzene, 1,2,4-trimethylbenzene, ethyl benzene, toluene, o-, p-, and m-xylene, methanol,

476   and C_2H_2).

477   OH reactivity varied substantially at the two sites in both magnitude and relative

478   importance of the individual constituents. Overall, average afternoon OH reactivity at UTSA

479   and Floresville were 12 and 4.0 s^{-1}, respectively. While the main contributors to OH reactivity

480   varied between morning and afternoon at both sites, the total reactivity did not show significant

481   variation. The higher OH reactivity at UTSA is consistent with the higher $P(O_3)$ rate and XO_2

482   concentrations. At UTSA, the predominant contributors to OH reactivity were NO_X in the

483   morning and biogenic VOCs in the afternoon, comprising 46% and 55% of OH reactivity,

484   respectively. Isoprene dominated the biogenic contribution, with less than 10% of total OH

485   reactivity resulting from monoterpenes, which have been assumed to be 100% α-pinene.

486   Although the contribution of biogenic VOCs was lower at Floresville than at UTSA, they were

487   still the largest component of OH reactivity in the afternoon. The significant contribution to OH

488   reactivity from NO_X during the morning is consistent with large on-road emissions and a low

489   boundary layer as well as with the VOC-limited nature of O_3 production in the morning. During

490   these morning hours, when the region is VOC-limited and $P(RO_X)$ is generally less than 0.2

491   pptv/s, NO can frequently exceed 500 pptv (Fig. 6c), as compared to the campaign median of

492   225 pptv. CO and carbonyls were the other major contributors to OH reactivity at all locations,

493   with CO being the dominant contributor at Floresville in the morning. Because one of the

494   dominant contributors to HCHO production is isoprene (Wolfe et al., 2016a), it is likely that the

495   biogenic contribution to OH reactivity is even higher than indicated here. Contributions from

496   alkanes were unimportant at the UTSA site, 1% or less during both morning and afternoon, and

497   contributed only 4-5% at Floresville.

498   The uncertainty in the isoprene measurements does not significantly alter the conclusions

499   presented here. To bound the effect of this uncertainty, we adjusted the isoprene observations by

500   $\pm$ 32% and recalculated the OH reactivity. This results in a range of $10.5 - 13.4$ and $3.8 - 4.3$

501   s^{-1} in total afternoon OH reactivity at UTSA and Floresville, respectively. NO_X remains the

502   dominant contributor at UTSA in the morning. For the lower bound, isoprene contributes 49%

503   of total OH reactivity at UTSA, by far the largest contributor to afternoon OH reactivity, and

504   23% at Floresville, making it second in importance to CO (25%).

505   Because of the large contribution of alkenes to OH reactivity at other Texas sites (Mao et

506   al., 2010), it is necessary to make an estimate of their importance during SAFS. With the

507   exception of isoprene and monoterpenes, alkenes were not measured onboard the AML and

508   therefore have not been included in the above analysis. To estimate the impact of anthropogenic

509   alkenes on OH reactivity, we include in our calculation of OH reactivity observations of alkenes

510   made at nearby TCEQ monitoring sites, Camp Bullis for UTSA and a site in Floresville co-

511   located with the AML. These sites provide hourly observations of cis-2-butene, trans-2-butene,

512   1-pentene, cis-2-pentene, trans-2-pentene, ethene, propene, 1,3-butadiene, and 1-butene. Alkene

513   concentrations at the SAFS monitoring sites were assumed to be identical to those at the TCEQ

514   monitoring sites and were interpolated to the ECHAMP time base. This assumption is likely

515   more accurate for the Floresville site than for UTSA. A regression of hourly averaged *n*-pentane

516   measured onboard the AML to that measured at the Camp Bullis TCEQ site has an r^2 of 0.3,

517 even after maximizing the correlation using a lead-lag analysis. In addition, the maximum *n*-

518 pentane concentrations at the Camp Bullis site are almost a factor of 2 higher than those seen at

519 UTSA. Regressions of cyclohexane and benzene between the two sites show even lower r^2

520 values. On the other hand, a similar regression of n-pentane at the Floresville site has an r^2 of

521 0.83. Better agreement at Floresville is to be expected since the AML and TCEQ monitor were

522 co-located.   Total OH reactivity was then recalculated using the estimates of alkene

523 concentrations. Alkenes contribute less than 1% of total reactivity at both UTSA and Floresville

524 for morning and afternoon times.

525 *4. Discussion and conclusions*

526   We have presented observations of O_3, its precursors, and total observations of XO_2 at

527 three sites in the San Antonio region. We also presented determinations of $P(O_3)$ calculated from

528 measurements of total peroxy radicals. Median daytime $P(O_3)$ at UTSA was 4.1 ppbv hr^{-1},

529 compared to just over 1 ppbv hr^{-1} at the other two SAFS sites. Ozone production rates at UTSA

530 were still far lower, however, than values observed during campaigns in Houston. Mazzuca et

531 al. (2016) found median near surface gross $P(O_3)$ of about 10 ppbv hr^{-1} during the DISCOVER-

532 AQ campaign in the summer of 2013, with values up to 140 ppbv hr^{-1} seen over the Houston

533 shipping channel. These values are consistent with previous studies in the region (Sommariva et

534 al., 2011). Higher concentrations of NO and larger production rates of RO_X were seen during

535 DISCOVER-AQ than during SAFS, both of which could lead to higher $P(O_3)$.

536   During SAFS, ozone peaked at UTSA at 80 ppbv, with a median value of 47 ppbv,

537 almost 20 ppbv higher than at the background site of Floresville, upwind of San Antonio. Along

538 with higher O_3, the UTSA site also had larger $P(O_3)$, isoprene, NO, and XO_2 concentrations than

539 upwind sites. Differences in [O_3] between the up- and downwind sites could be the result of the

540   effects of urban emissions on O_3 production, or they could result from daily variability, since

541   simultaneous observations were not made at both sites and there are no permanent O_3

542   observations at Floresville. Figure S5 compares O_3 observations from the AML while at UTSA

543   to those made by the University of Houston (UH), who measured O_3 continuously at UTSA

544   during SAFS, and to observations from the TCEQ sites at Lake Calaveras, located upwind of

545   downtown San Antonio (Fig. 2b), and Pecan Valley, situated in downtown San Antonio.

546   Between 17 and 30 May, winds in the San Antonio region were primarily southeasterly (*i.e.* they

547   travelled in the general direction from Lake Calaveras to UTSA, with downtown San Antonio in-

548   between). During this period, there are both days where O_3 is almost identical at all sites and

549   where O_3 is 20 ppbv higher at UTSA than at Lake Calaveras, suggesting significant O_3

550   production in the air as it travelled between the two sites. These results suggest that the 20 ppbv

551   differences in median values between the UTSA and Floresville sites could be either the result of

552   day-to-day variability, *in situ* O_3 production as the air travelled between the two sites, or a

553   mixture of the two. Further observations of O_3 and its precursors in the region, including in

554   downtown San Antonio, are needed to fully characterize the effects of the city on ozone

555   production. In addition, future modeling studies will investigate the evolution of ozone

556   production during this campaign.

557   A variety of methods were used to show that with the exception of early morning, when

558   NO is high and XO_2 concentrations are low due to limited insolation, ozone production at the

559   three SAFS sites is NO_X-limited. The relationship between $P(O_3)$ and NO was consistent at the

560   three sites, although the lower $P(RO_X)$, NO, and VOC reactivity at Floresville and Corpus Christi

561   led to overall lower ozone production rates as compared to UTSA. VOC-limited points

562   comprised only 20% of total daytime observations and generally had $P(O_3)$ less than 5 ppbv hr^{-1}

563   at UTSA and less than 2 ppbv hr^{-1} at the other two sites. This diurnal cycle is in agreement with

564   observations made in Houston during the DISCOVER-AQ (Mazzuca et al., 2016) and SHARP

565   (Ren et al., 2013) campaigns. These results, however, are limited to the examined time period

566   and location, but comparison to O_3 and NO levels at the Camp Bullis site suggests the

567   observations at UTSA are typical for an area downwind of the San Antonio urban center. This is

568   in contrast, however, to observations at the TCEQ Pecan Valley site which has not had an ozone

569   exceedance day by either EPA standard since 2015 but regularly has MDA8 NO greater than 50

570   ppbv, significantly larger than the maximum 2-minute value of 4 ppbv seen at the UTSA site.

571   Mixing ratios of O_X at Pecan Valley and Camp Bullis (Fig. 1) are essentially identical,

572   suggesting that there is less O_3 titration downwind of central San Antonio than in the urban core.

573   Given the higher [NO_X] in the urban core of San Antonio, P(O_3) could be significantly different

574   than at the UTSA site.   Supporting this idea of variations in ozone production across the San

575   Antonio region is the time series of O_3 at Pecan Valley, UTSA, and Lake Calaveras during SAFS

576   (Fig. S5). Ozone concentrations are frequently lower at this site than at both UTSA and Lake

577   Calaveras, despite its location downwind of Lake Calaveras.

578   OH reactivity at UTSA was found to be 12 s^{-1}, with the primary contributor being

579   isoprene. While the overall magnitude of the reactivity was comparable to that observed and

580   modeled during the TRAMP2006 campaign in Houston (Mao et al., 2010), the contributors to

581   OH reactivity were found to be significantly different. Contributions from aromatics were

582   negligible at UTSA while they were found to be 15% during TRAMP2006. In Houston,

583   anthropogenic alkenes were found to be responsible for 20-30% of total reactivity, with biogenic

584   VOCs making up less than 10%. Here, biogenic VOCs were responsible for 55% of total

585   daytime reactivity, with alkenes making up less than 1%, although alkene values were based on

586   estimates from a different site. We caution that this result cannot necessarily be extrapolated to

587   other areas in the San Antonio region. Isoprene has a lifetime on the order of an hour, and the

588   high biogenic contribution to OH reactivity seen here could result from local influences. While

589   there are trees throughout the San Antonio region, the results at UTSA cannot be extrapolated to

590   areas with far less foliage without further observations. Other VOCs could comprise a larger

591   fraction of total OH reactivity in less vegetated areas.

592   While the isoprene concentration at Floresville was significantly lower than at UTSA, it

593   was still the dominant contributor to OH reactivity during the afternoon, although the total OH

594   reactivity was a factor of 3 lower at this site ($4\ s^{-1}$) than at UTSA. Schade and Roest (2016)

595   found a significantly different OH reactivity profile at Floresville than described here, with

596   alkanes accounting for approximately 70% of total OH reactivity, with biogenic VOCs

597   contributing less than 5%. Observed isoprene at Floresville during SAFS was more than an order

598   of magnitude larger than that reported in Schade and Roest (2016), with alkane concentrations

599   consistent between the two studies. When the data used in Schade and Roest (2016) are subset to

600   afternoon times and May through July, the contribution of isoprene to VOC reactivity increases

601   to a median value of 38%, in agreement with the results presented here (Schade, personal

602   communication). The differences between the two studies do suggest that there could be

603   significant seasonal and diurnal variations in OH reactivity. Nevertheless, these results suggest

604   that policies designed to limit O_3 production at the SAFS sites discussed here should initially

605   focus primarily on NO_x reductions as the region is NO_x limited and the primary VOC

606   contributor is biogenic. Further observations and analysis are need to determine whether this

607   holds true in the urban core of downtown San Antonio.

608   *5. Data Availability*

609

610   Data from SAFS are maintained on a private server but are available upon request to the

611 authors.

612
613 *6. Author Contributions*
614
615   D.CA. and E.W wrote the manuscript. All authors discussed the results and commented

616 on the manuscript. All authors also contributed to daily running of the AML. S.C.H. led the

617 campaign. D.C.A., J.P, and E.C.W. measured XO_2. B.M.L. and W.B.K. contributed to the

618 measurement of organic trace gases. J.R.R., T.I.Y., and S.C.H. led observations with TILDAS

619 instruments as well as measurements of NO, NO_2, and O_3.

620
621 *7. Competing Interests*
622
623   The authors declare no competing interests.
624
625 *8. Acknowledgements*
626

627   The authors acknowledge support from NSF grants AGS-1443842 and AGS-1719918. In

628 addition, this research was funded by a grant (project 17-032) from the Texas Air Quality

629 Research Program (AQRP) at the University of Texas Austin through the Texas Emission

630 Reduction Program (TERP) and the Texas Commission on Environmental Quality (TCEQ). The

631 findings, opinions, and conclusions are the work of the authors and do not necessarily represent

632 the findings, opinions, or conclusions of the AQRP or the TCEQ. The authors thank S. Hall and

633 K. Ullmann of NCAR, J. Flynn of the University of Houston, D. Sullivan of the University of

634 Texas at Austin, and R. Nadkarni and M. Estes of TCEQ for their contributions to the SAFS

635 campaign and this paper.

636

9. References

639 Bell, M. L., Peng, R. D., and Dominici, F.: The exposure-response curve for ozone and risk of mortality
640 and the adequacy of current ozone regulations, Environmental Health Perspectives, 114, 532-536,
641 10.1289/ehp.8816, 2006.

642 Bucsela, E. J., Krotkov, N. A., Celarier, E. A., Lamsal, L. N., Swartz, W. H., Bhartia, P. K., Boersma, K.
643 F., Veefkind, J. P., Gleason, J. F., and Pickering, K. E.: A new stratospheric and tropospheric
644 NO_2 retrieval algorithm for nadir-viewing satellite instruments: applications to OMI, Atmos.
645 Meas. Tech., 6, 2607-2626, 10.5194/amt-6-2607-2013, 2013.

646 Choi, Y., and Souri, A. H.: Chemical condition and surface ozone in large cities of Texas during the last
647 decade: Observational evidence from OMI, CAMS, and model analysis, Remote Sensing of Environment,
648 168, 90-101, 10.1016/j.rse.2015.06.026, 2015.

649 Cooper, O. R., Gao, R.-S., Tarasick, D., Leblanc, T., and Sweeney, C.: Long-term ozone trends at rural
650 ozone monitoring sites across the United States, 1990-2010, Journal of Geophysical Research:
651 Atmospheres, 117, n/a-n/a, 10.1029/2012jd018261, 2012.

652 Duncan, B. N., Yoshida, Y., Olson, J. R., Sillman, S., Martin, R. V., Lamsal, L., Hu, Y., Pickering, K. E.,
653 Retscher, C., Allen, D. J., and Crawford, J. H.: Application of OMI observations to a space-based
654 indicator of NOx and VOC controls on surface ozone formation, Atmospheric Environment, 44, 2213-
655 2223, 10.1016/j.atmosenv.2010.03.010, 2010.

656 Duncan, B. N., Lamsal, L. N., Thompson, A. M., Yoshida, Y., Lu, Z. F., Streets, D. G., Hurwitz, M. M.,
657 and Pickering, K. E.: A space-based, high-resolution view of notable changes in urban NOx pollution
658 around the world (2005-2014), Journal of Geophysical Research-Atmospheres, 121, 976-996,
659 10.1002/2015jd024121, 2016.

660 EPA: National Ambient Air Quality Standards for Ozone, Federal Register, 80, 2015.

661 Faloona, I. C., Tan, D., Lesher, R. L., Hazen, N. L., Frame, C. L., SImpas, J. B., Harder, G., Martinez, M.,
662 Di Carlo, P., Ren, X., and Brune, W. H.: A Laser-induced Fluorescence Instrument for Detecting
663 Tropospheric OH and HO2: Characteristics and Calibration, Journal of Atmospheric Chemistry, 47, 139-
664 167, 2004.

665 González Abad, G., Liu, X., Chance, K., Wang, H., Kurosu, T. P., and Suleiman, R.: Updated
666 Smithsonian Astrophysical Observatory Ozone Monitoring Instrument (SAO OMI) formaldehyde
667 retrieval, Atmospheric Measurement Techniques, 8, 19-32, 10.5194/amt-8-19-2015, 2015.

668 He, H., Stehr, J. W., Hains, J. C., Krask, D. J., Doddridge, B. G., Vinnikov, K. Y., Canty, T. P., Hosley,
669 K. M., Salawitch, R. J., Worden, H. M., and Dickerson, R. R.: Trends in emissions and concentrations of
670 air pollutants in the lower troposphere in the Baltimore/Washington airshed from 1997 to 2011,
671 Atmospheric Chemistry and Physics, 13, 7859-7874, 10.5194/acp-13-7859-2013, 2013.

672 Herndon, S. C., Jayne, J. T., Zahniser, M. S., Worsnop, D. R., Knighton, B., Alwine, E., Lamb, B. K.,
673 Zavala, M., Nelson, D. D., McManus, J. B., Shorter, J. H., Canagaratna, M. R., Onasch, T. B., and Kolb,
674 C. E.: Characterization of urban pollutant emission fluxes and ambient concentration distributions using a

675   mobile laboratory with rapid response instrumentation, Faraday Discussions, 130, 327-339,
676   10.1039/b500411j, 2005.

677   Holton, J. R., Haynes, P. H., McIntyre, M. E., Douglass, A. R., Rood, R. B., and Pfister, L.: Stratosphere-
678   Troposphere Exchange, Reviews of Geophysics, 33, 403-439, 1995.

679   Jerrett, M., Burnett, R. T., Pope, C. A., Ito, K., Thurston, G., Krewski, D., Shi, Y. L., Calle, E., and Thun,
680   M.: Long-Term Ozone Exposure and Mortality, New England Journal of Medicine, 360, 1085-1095,
681   10.1056/NEJMoa0803894, 2009.

682   Kebabian, P. L., Herndon, S. C., and Freedman, A.: Detection of Nitrogen Dioxide by Cavity Attenuated
683   Phase Shift Spectroscopy, Analytical Chemistry, 77, 724-728, 10.1029/, 2005.

684   Kebabian, P. L., Wood, E. C., Herndon, S. C., and Freedman, A.: A Practical Alternative to
685   Chemiluminescence-Based Detection of Nitrogen Dioxide: Cavity Attenuated Phase Shift Spectroscopy,
686   Environmental Science & Technology, 42, 6040-6045, 2008.

687   Kleinman, L. I.: LOW AND HIGH NOX TROPOSPHERIC PHOTOCHEMISTRY, Journal of
688   Geophysical Research-Atmospheres, 99, 16831-16838, 10.1029/94jd01028, 1994.

689   Kleinman, L. I., Daum, P. H., Imre, D., Lee, Y. N., Nunnermacker, L. J., Springston, S. R., Weinstein-
690   Lloyd, J., and Rudolph, J.: Ozone production rate and hydrocarbon reactivity in 5 urban areas: A cause of
691   high ozone concentration in Houston, Geophysical Research Letters, 29, 105-101-105-104,
692   10.1029/2001gl014569, 2002.

693   Kleinman, L. I.: The dependence of tropospheric ozone production rate on ozone precursors, Atmospheric
694   Environment, 39, 575-586, 10.1016/j.atmosenv.2004.08.047, 2005.

695   Krotkov, N. A., Lamsal, L. N., Celarier, E. A., Swartz, W. H., Marchenko, S. V., Bucsela, E. J., Chan, K.
696   L., Wenig, M., and Zara, M.: The version 3 OMI NO2 standard product, Atmospheric Measurement
697   Techniques, 10, 3133-3149, 10.5194/amt-10-3133-2017, 2017.

698   Kundu, S., Deming, B. L., Lew, M. M., Bottorff, B. P., Rickly, P., Stevens, P. S., Dusanter, S., Sklaveniti,
699   S., Leonardis, T., Locoge, N., and Wood, E. C.: Peroxy Radical Measurements by Ethane – Nitric Oxide
700   Chemical Amplification and Laser-Induced Fluorescence/Fluorescence Assay by Gas Expansion during
701   the IRRONIC field campaign in a Forest in Indiana, Atmos. Chem. Phys. Discuss., 2019, 1-31,
702   10.5194/acp-2018-1359, 2019.

703   Lamarque, J. F., Hess, P., Emmons, L., Buja, L., Washington, W., and Granier, C.: Tropospheric ozone
704   evolution between 1890 and 1990, Journal of Geophysical Research-Atmospheres, 110,
705   10.1029/2004jd005537, 2005.

706   Lamsal, L. N., Duncan, B. N., Yoshida, Y., Krotkov, N. A., Pickering, K. E., Streets, D. G., and Lu, Z. F.:
707   U.S. NO2 trends (2005-2013): EPA Air Quality System (AQS) data versus improved observations from
708   the Ozone Monitoring Instrument (OMI), Atmospheric Environment, 110, 130-143,
709   10.1016/j.atmosenv.2015.03.055, 2015.

710   Lee, B. H., Wood, E. C., Herndon, S. C., Lefer, B. L., Luke, W. T., Brune, W. H., Nelson, D. D.,
711   Zahniser, M. S., and Munger, J. W.: Urban measurements of atmospheric nitrous acid: A caveat on the
712   interpretation of the HONO photostationary state, Journal of Geophysical Research: Atmospheres, 118,
713   12,274-212,281, 10.1002/2013jd020341, 2013.

714 Mao, J. Q., Ren, X., Chen, S., Brune, W. H., Chen, Z., Martinez, M., Harder, H., Lefer, B., Rappenglück,
715 B., Flynn, J., and Leuchner, M.: Atmospheric oxidation capacity in the summer of Houston 2006:
716 Comparison with summer measurements in other metropolitan studies, Atmospheric Environment, 44,
717 4107-4115, 10.1016/j.atmosenv.2009.01.013, 2010.

718 Mazzuca, G. M., Ren, X., Loughner, C. P., Estes, M., Crawford, J. H., Pickering, K. E., Weinheimer, A.
719 J., and Dickerson, R. R.: Ozone production and its sensitivity to NOx and VOCs: results from the
720 DISCOVER-AQ field experiment, Houston 2013, Atmospheric Chemistry and Physics, 16, 14463-14474,
721 10.5194/acp-16-14463-2016, 2016.

722 McManus, J. B., Zahniser, M. S., Nelson, D. D., Shorter, J. H., Herndon, S. C., Jervis, D., Agnese, M.,
723 McGovern, R., Yacovitch, T. I., and Roscioli, J. R.: Recent progress in laser-based trace gas instruments:
724 performance and noise analysis, Applied Physics B-Lasers and Optics, 119, 203-218, 10.1007/s00340-
725 015-6033-0, 2015.

726 Mihele, C. M., and Hastie, D. R.: Optimized operation and calibration procedures for radical amplifier-
727 type detectors, Journal of Atmospheric and Oceanic Technology, 17, 788-794, 10.1175/1520-
728 0426(2000)017<0788:Ooacpf>2.0.Co;2, 2000.

729 Orlando, J. J., and Tyndall, G. S.: Laboratory studies of organic peroxy radical chemistry: an overview
730 with emphasis on recent issues of atmospheric significance, Chemical Society Reviews, 41, 6294-6317,
731 10.1039/c2cs35166h, 2012.

732 Park, S. K., O'Neill, M. S., Vokonas, P. S., Sparrow, D., and Schwartz, J.: Effects of air pollution on heart
733 rate variability: The VA Normative Aging Study, Environmental Health Perspectives, 113, 304-309,
734 10.1289/ehp.7447, 2005.

735 Pollack, I. B., Ryerson, T. B., Trainer, M., Parrish, D. D., Andrews, A. E., Atlas, E. L., Blake, D. R.,
736 Brown, S. S., Commane, R., Daube, B. C., de Gouw, J. A., Dubé, W. P., Flynn, J., Frost, G. J., Gilman, J.
737 B., Grossberg, N., Holloway, J. S., Kofler, J., Kort, E. A., Kuster, W. C., Lang, P. M., Lefer, B., Lueb, R.
738 A., Neuman, J. A., Nowak, J. B., Novelli, P. C., Peischl, J., Perring, A. E., Roberts, J. M., Santoni, G.,
739 Schwarz, J. P., Spackman, J. R., Wagner, N. L., Warneke, C., Washenfelder, R. A., Wofsy, S. C., and
740 Xiang, B.: Airborne and ground-based observations of a weekend effect in ozone, precursors, and
741 oxidation products in the California South Coast Air Basin, Journal of Geophysical Research:
742 Atmospheres, 117, n/a-n/a, 10.1029/2011jd016772, 2012.

743 Pollmann, J., Helmig, D., Hueber, J., Tanner, D., and Tans, P. P.: Evaluation of solid adsorbent materials
744 for cryogen-free trapping - gas chromatographic analysis of atmospheric C2-C6 non-methane
745 hydrocarbons, Journal of Chromatography A, 1134, 1-15, 10.1016/j.chroma.2006.08.050, 2006.

746 Ren, X., van Duin, D., Cazorla, M., Chen, S., Mao, J., Zhang, L., Brune, W. H., Flynn, J. H., Grossberg,
747 N., Lefer, B. L., Rappenglück, B., Wong, K. W., Tsai, C., Stutz, J., Dibb, J. E., Thomas Jobson, B., Luke,
748 W. T., and Kelley, P.: Atmospheric oxidation chemistry and ozone production: Results from SHARP
749 2009 in Houston, Texas, Journal of Geophysical Research: Atmospheres, 118, 5770-5780,
750 10.1002/jgrd.50342, 2013.

751 Ring, A. M., Canty, T. P., Anderson, D. C., Vinciguerra, T. P., He, H., Goldberg, D. L., Ehrman, S. H.,
752 Dickerson, R. R., and Salawitch, R. J.: Evaluating commercial marine emissions and their role in air
753 quality policy using observations and the CMAQ model, Atmospheric Environment, 173, 96-107,
754 10.1016/j.atmosenv.2017.10.037, 2018.

Ryerson, T. B., Trainer, M., Angevine, W. M., Brock, C. A., Dissly, R. W., Fehsenfeld, F. C., Frost, G. J., Goldan, P. D., Holloway, J. S., Hubler, G., Jakoubek, R. O., Kuster, W. C., Neuman, J. A., Nicks, D. K., Parrish, D. D., Roberts, J. M., Sueper, D. T., Atlas, E. L., Donnelly, S. G., Flocke, F., Fried, A., Potter, W. T., Schauffler, S., Stroud, V., Weinheimer, A. J., Wert, B. P., Wiedinmyer, C., Alvarez, R. J., Banta, R. M., Darby, L. S., and Senff, C. J.: Effect of petrochemical industrial emissions of reactive alkenes and NOx on tropospheric ozone formation in Houston, Texas, Journal of Geophysical Research-Atmospheres, 108, 10.1029/2002jd003070, 2003.

Sanchez, J., Tanner, D. J., Chen, D., Huey, L. G., and Ng, N. L.: A new technique for the direct detection of HO_2 radicals using bromide chemical ionization mass spectrometry (Br-CIMS): initial characterization, Atmospheric Measurement Techniques, 9, 3851-3861, 10.5194/amt-9-3851-2016, 2016.

Sanders, S. P., Friedl, R. R., Abbatt, J. P. D., Barker, J. R., Burkholder, J. B., Golden, D. M., Kolb, C. E., Kurylo, M. J., Moortgat, G. K., Wine, P. H., R.E., H., and Orkin, V. L.: Chemical Kinetics and Photochemical Data for Use in Atmopsheric Studies, 2011.

Schade, G. W., and Roest, G.: Analysis of non-methane hydrocarbon data from a monitoring station affected by oil and gas development in the Eagle Ford shale, Texas, Elementa: Science of the Anthropocene, 4, 10.12952/journal.elementa.000096, 2016.

Schroeder, J. R., Crawford, J. H., Fried, A., Walega, J., Weinheimer, A., Wisthaler, A., Müller, M., Mikoviny, T., Chen, G., Shook, M., Blake, D. R., and Tonnesen, G. S.: New insights into the column CH2O/NO2 ratio as an indicator of near-surface ozone sensitivity, Journal of Geophysical Research: Atmospheres, 10.1002/2017jd026781, 2017.

Shetter, R. E., Junkermann, W., Swartz, W. H., Frost, G. J., Crawford, J. H., Lefer, B. L., Barrick, J. D., Hall, S. R., Hofzumahaus, A., Bais, A., Calvert, J. G., Cantrell, C. A., Madronich, S., Muller, M., Kraus, A., Monks, P. S., Edwards, G. D., McKenzie, R., Johnston, P., Schmitt, R., Griffioen, E., Krol, M., Kylling, A., Dickerson, R. R., Lloyd, S. A., Martin, T., Gardiner, B., Mayer, B., Pfister, G., Roth, E. P., Koepke, P., Ruggaber, A., Schwander, H., and van Weele, M.: Photolysis frequency of NO2: Measurement and modeling during the International Photolysis Frequency Measurement and Modeling Intercomparison (IPMMI), Journal of Geophysical Research-Atmospheres, 108, 10.1029/2002jd002932, 2003.

Silva, R. A., West, J. J., Zhang, Y., Anenberg, S. C., Lamarque, J.-F., Shindell, D. T., Collins, W. J., Dalsoren, S., Faluvegi, G., Folberth, G., Horowitz, L. W., Nagashima, T., Naik, V., Rumbold, S., Skeie, R., Sudo, K., Takemura, T., Bergmann, D., Cameron-Smith, P., Cionni, I., Doherty, R. M., Eyring, V., Josse, B., MacKenzie, I. A., Plummer, D., Righi, M., Stevenson, D. S., Strode, S., Szopa, S., and Zeng, G.: Global premature mortality due to anthropogenic outdoor air pollution and the contribution of past climate change, Environmental Research Letters, 8, 034005, 10.1088/1748-9326/8/3/034005, 2013.

Sommariva, R., Brown, S. S., Roberts, J. M., Brookes, D. M., Parker, A. E., Monks, P. S., Bates, T. S., Bon, D., de Gouw, J. A., Frost, G. J., Gilman, J. B., Goldan, P. D., Herndon, S. C., Kuster, W. C., Lerner, B. M., Osthoff, H. D., Tucker, S. C., Warneke, C., Williams, E. J., and Zahniser, M. S.: Ozone production in remote oceanic and industrial areas derived from ship based measurements of peroxy radicals during TexAQS 2006, Atmospheric Chemistry and Physics, 11, 2471-2485, 10.5194/acp-11-2471-2011, 2011.

Stark, H., Lerner, B. M., Schmitt, R., Jakoubek, R., Williams, E. J., Ryerson, T. B., Sueper, D. T., Parrish, D. D., and Fehsenfeld, F. C.: Atmospheric in situ measurement of nitrate radical (NO3) and other photolysis rates using spectroradiometry and filter radiometry, Journal of Geophysical Research-Atmospheres, 112, 10.1029/2006jd007578, 2007.

798 Thornton, J. A.: Ozone production rates as a function of NOx abundances and HOx production rates in
799 the Nashville urban plume, Journal of Geophysical Research, 107, 10.1029/2001jd000932, 2002.

800 Whalley, L. K., Stone, D., Dunmore, R., Hamilton, J., Hopkins, J. R., Lee, J. D., Lewis, A. C., Williams,
801 P., Kleffmann, J., Laufs, S., Woodward-Massey, R., and Heard, D. E.: Understanding in situ ozone
802 production in the summertime through radical observations and modelling studies during the Clean air for
803 London project (ClearfLo), Atmospheric Chemistry and Physics, 18, 2547-2571, 10.5194/acp-18-2547-
804 2018, 2018.

805 Wolfe, G. M., Kaiser, J., Hanisco, T. F., Keutsch, F. N., de Gouw, J. A., Gilman, J. B., Graus, M., Hatch,
806 C. D., Holloway, J., Horowitz, L. W., Lee, B. H., Lerner, B. M., Lopez-Hilifiker, F., Mao, J., Marvin, M.
807 R., Peischl, J., Pollack, I. B., Roberts, J. M., Ryerson, T. B., Thornton, J. A., Veres, P. R., and Warneke,
808 C.: Formaldehyde production from isoprene oxidation across NOx regimes, Atmospheric Chemistry and
809 Physics, 16, 2597-2610, 10.5194/acp-16-2597-2016, 2016a.

810 Wolfe, G. M., Marvin, M. R., Roberts, S. J., Travis, K. R., and Liao, J.: The Framework for 0-D
811 Atmospheric Modeling (F0AM) v3.1, Geosci. Model Dev., 9, 3309-3319, 10.5194/gmd-9-3309-2016,
812 2016b.

813 Wood, E. C., Deming, B. L., and Kundu, S.: Ethane-Based Chemical Amplification Measurement
814 Technique for Atmospheric Peroxy Radicals, Environmental Science & Technology Letters, 4, 15-19,
815 10.1021/acs.estlett.6b00438, 2017.
816
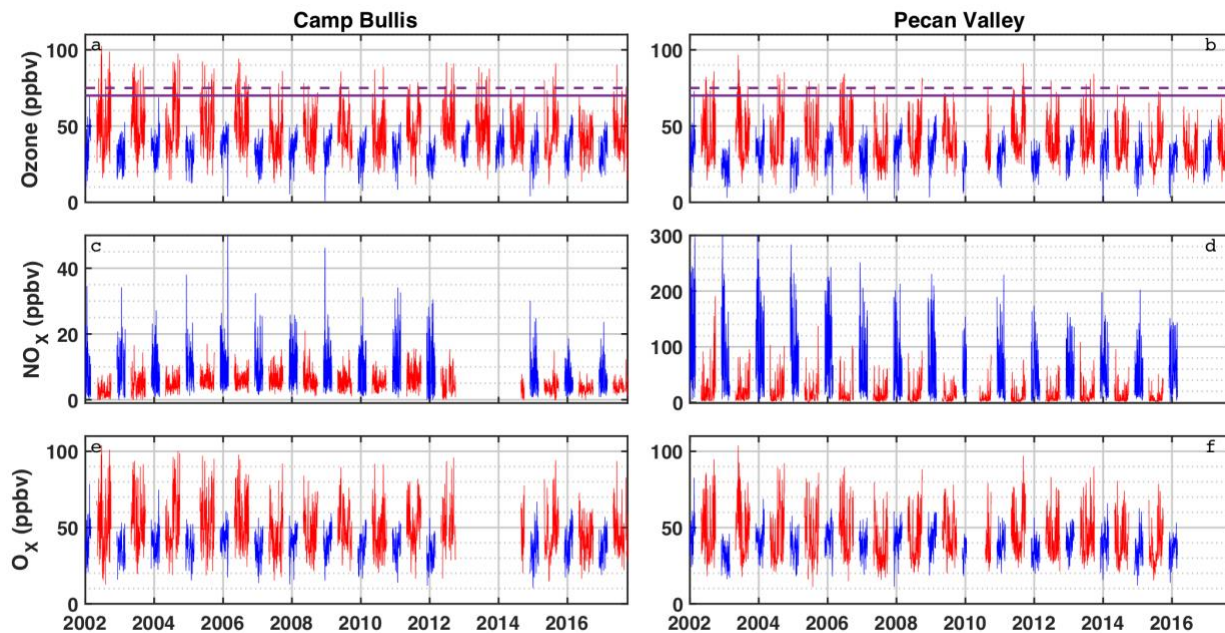
817

818 **Figure 1:** Time series of maximum daily average 8-hour (MDA8) O_3, NO_X, and O_X at the Camp
819 Bullis (**a**, **c**, **e**) and Pecan Valley (**b**, **d**, **f**) TCEQ sites for 2002 – 2017. Summer months (May –
820 September) are shown in red, and winter months (December – February) are shown in blue. MDA8
821 is calculated by determining the maximum value of a species from running 8 hour averages
822 throughout the day. The purple dashed and solid red lines represent the 2008 (75 ppbv) and 2015

823   (70   ppbv) O_3 standards   respectively.   Data   were   downloaded   from
824   www.tceq.texas.gov/goto/tamis.

825

826
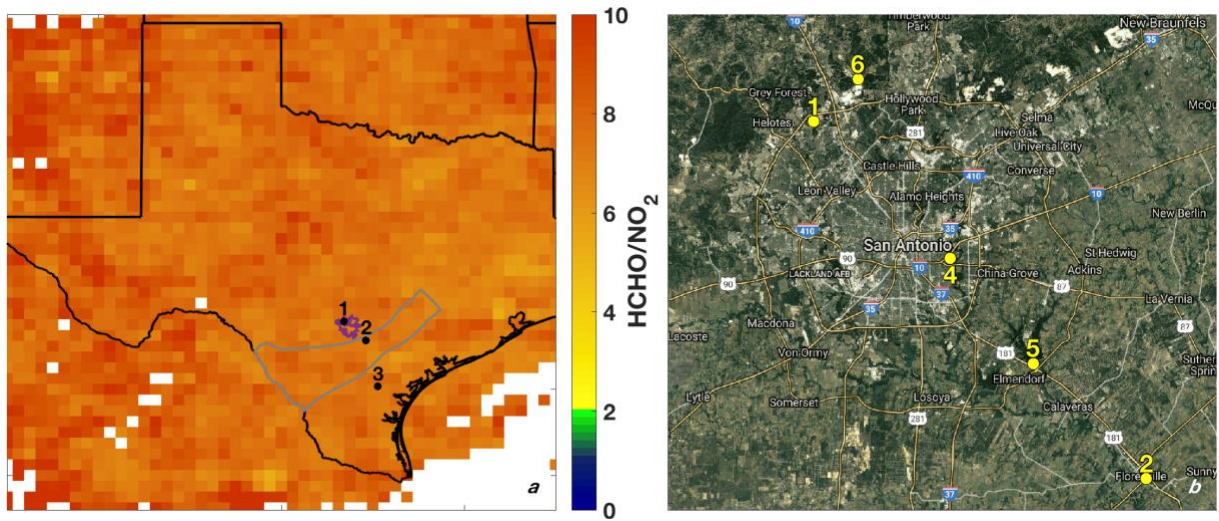
827
Figure 2: The sampling locations for the Aerodyne mobile laboratory are indicated: 1 – University of
Texas San Antonio, 2 – Floresville, 3 – Lake Corpus Christi. The ratio of total column HCHO to
tropospheric column NO_2 averaged over the months of May through July 2017 is also shown for grid
boxes with 10 or more observations of both species over the indicated time period. The outlines of the
Eagle Ford Shale (grey) play and San Antonio city limits (purple) are also shown for reference. (b) The
major roadways and TCEQ monitoring stations (6: Camp Bullis, 4: Pecan Valley, 5: Calaveras Lake) in
the San Antonio region used in this study are shown. The UTSA and Floresville SAFS sites are also
shown for reference.

836

837
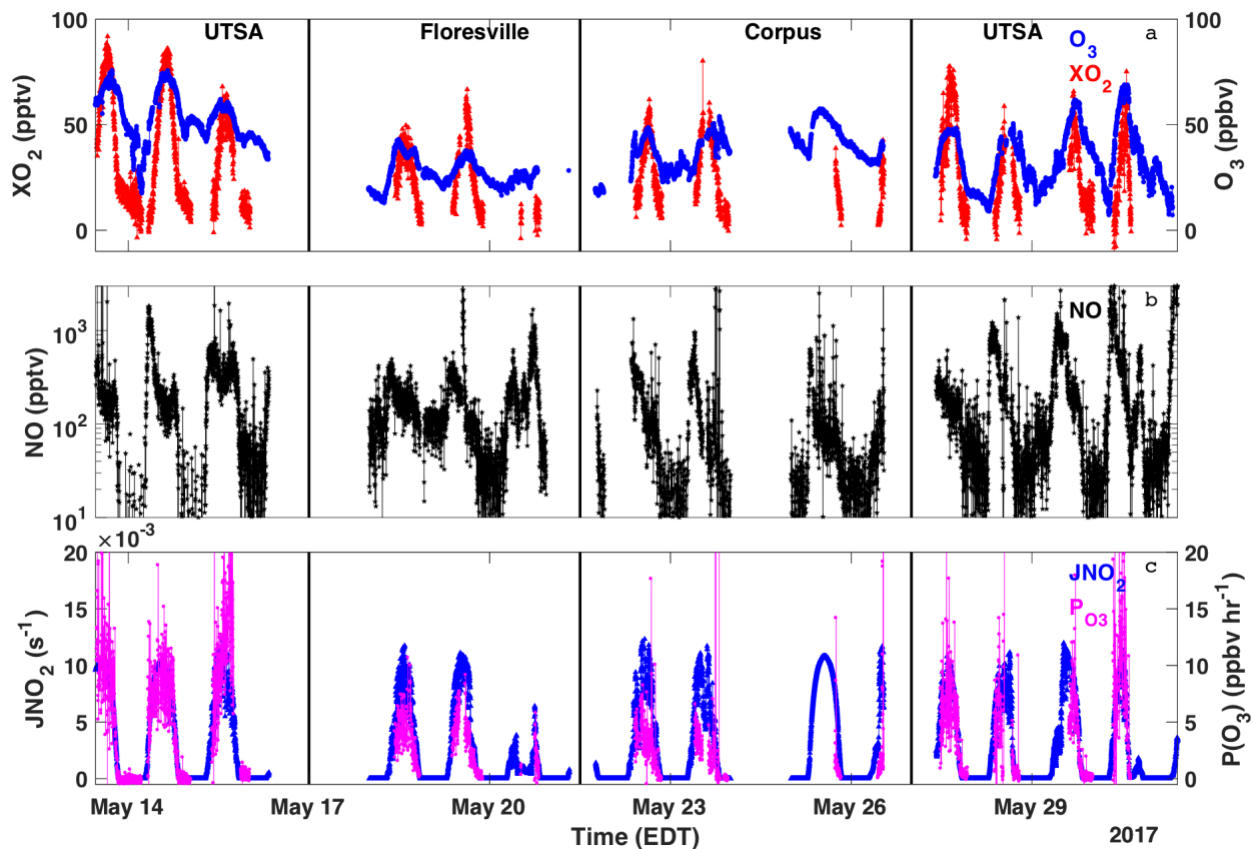
Figure 3: Time series of O_3 (blue circles), XO_2 (red triangles), NO (black stars), JNO_2 (blue triangles),
and $P(O_3)$ (magenta circles) measured at all sites. All data are averaged over the XO_2 sampling period.

840
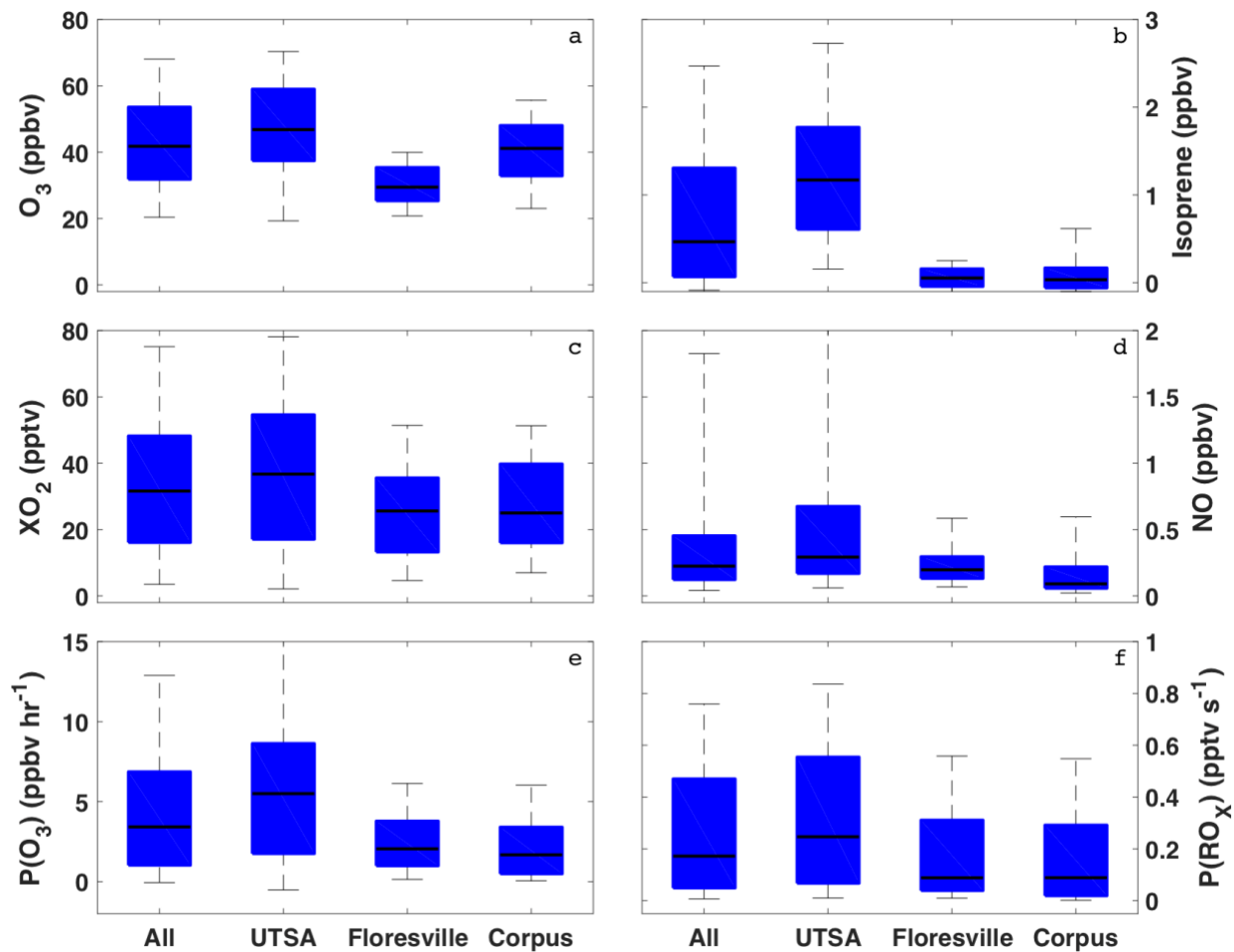
Figure 4: The distribution of O_3 (**a**), isoprene (**b**), XO_2 (**c**), NO (**d**), $P(O_3)$ (**e**), and $P(RO_X)$ (**f**) for all observations during SAFS taken between 07:00 and 20:00. The distribution for the entire campaign (All) as well as at the individual sites is shown. Medians are indicated by the black lines, and the 5th, 25th, 75th, and 95th percentiles are shown by the edges of the box and whiskers.

845
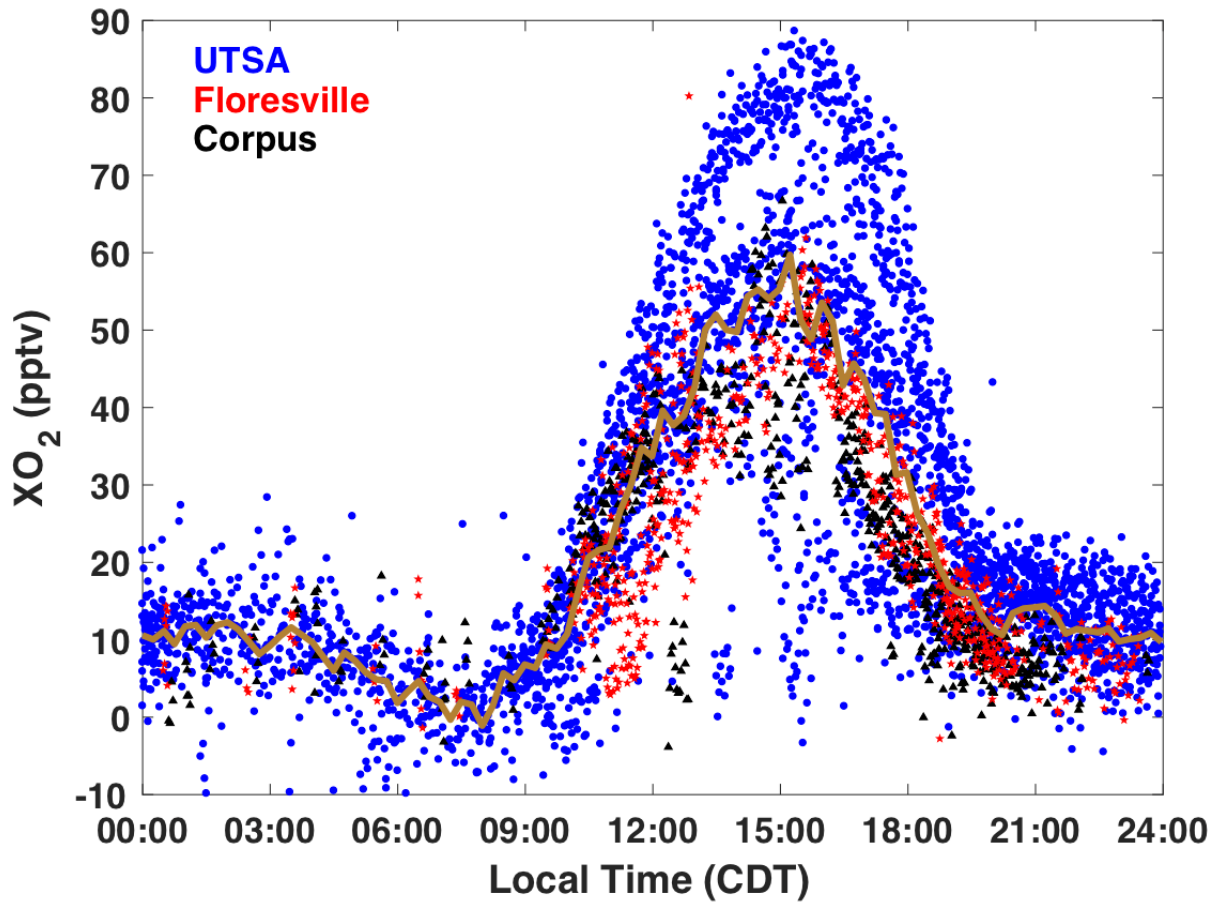
846

847 **Figure 5:** The diurnal profile of all 2 minute average XO_2 observations made during SAFS. Observations
848 made at UTSA are shown in blue, Floresville, in red, and Corpus, in black. The median value for 15-
849 minute time bins for observations at all sites is shown by the gold trace.

850

851

852

853

854
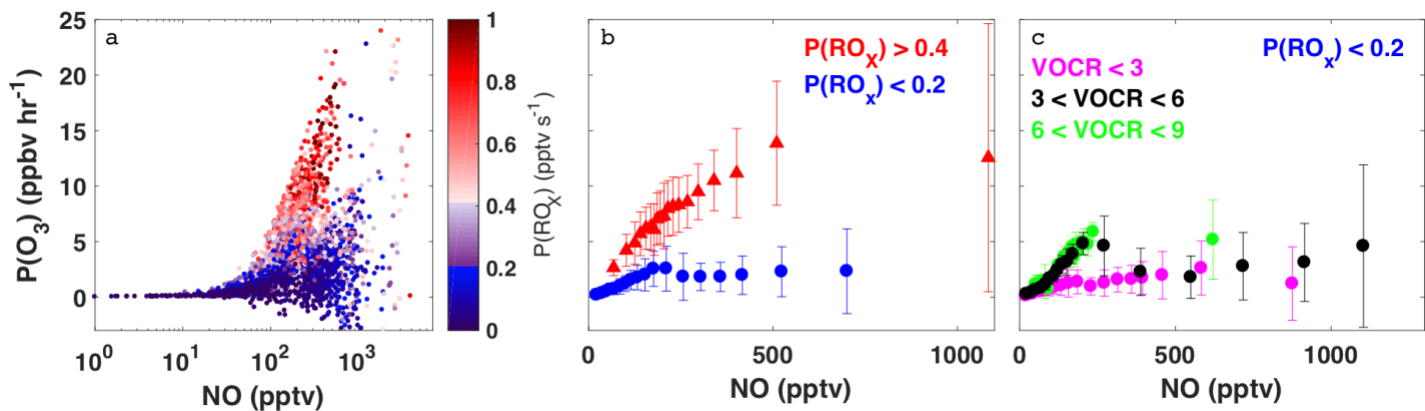
Figure 6: The variation of $P(O_3)$ with NO for all daytime observations (07:00 to 20:00) made during SAFS (**a**). Observations are colored by $P(RO_X)$. The same data as shown in panel (**a**) but sorted by $P(RO_X)$ are shown in panel (**b**). Observations with $P(RO_X)$ greater than 0.4 pptv s^{-1} are shown in red, while observations with $P(RO_X)$ less than 0.2 pptv s^{-1} are shown in blue. Data are separated into NO bins with an equal number of observations in bin. The mean value of each bin is shown, with the error bars showing one standard deviation. The subset of observations with $P(RO_X) < 0.2$ pptv s^{-1} are further separated into three categories: low VOC reactivity (VOCR < 3 s^{-1}; magenta), medium VOC reactivity (3 < VOCR < 6 s^{-1}; black), and high VOC reactivity (6 < VOCR < 9 s^{-1}; green) (**c**). As in panel (**b**) data are separated into NO bins with equal numbers of observations in each bin.

864
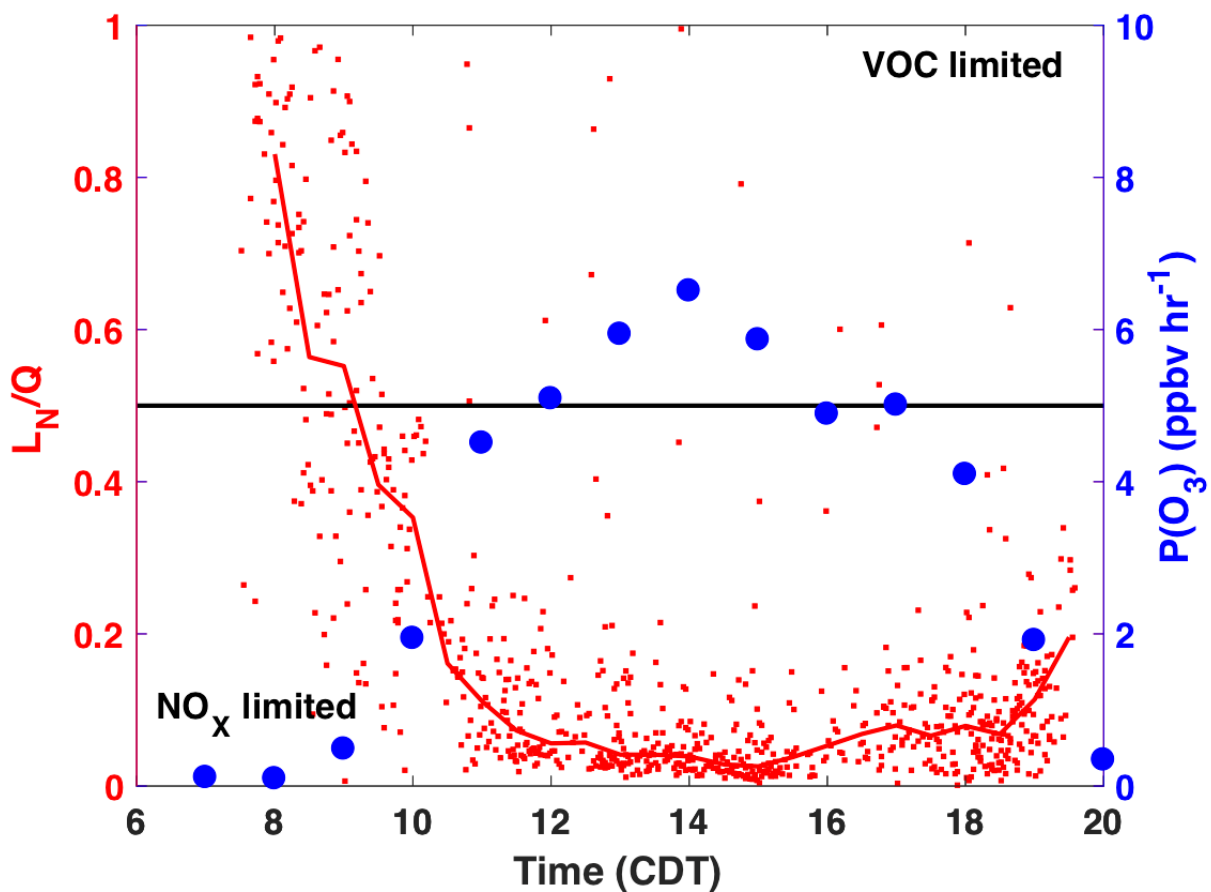
Figure 7: The diurnal profiles of L_N/Q calculated with the F0AM box model (red), and the median $P(O_3)$
in one hour time bins (blue). The median L_N/Q value for half hour bins is shown by the red line. Profiles
are only for observations at UTSA. Points are calculated by $P(O_3)$ calculated from observations. The
black line is approximately the separation between the NO_X- and VOC-limited regimes.

869
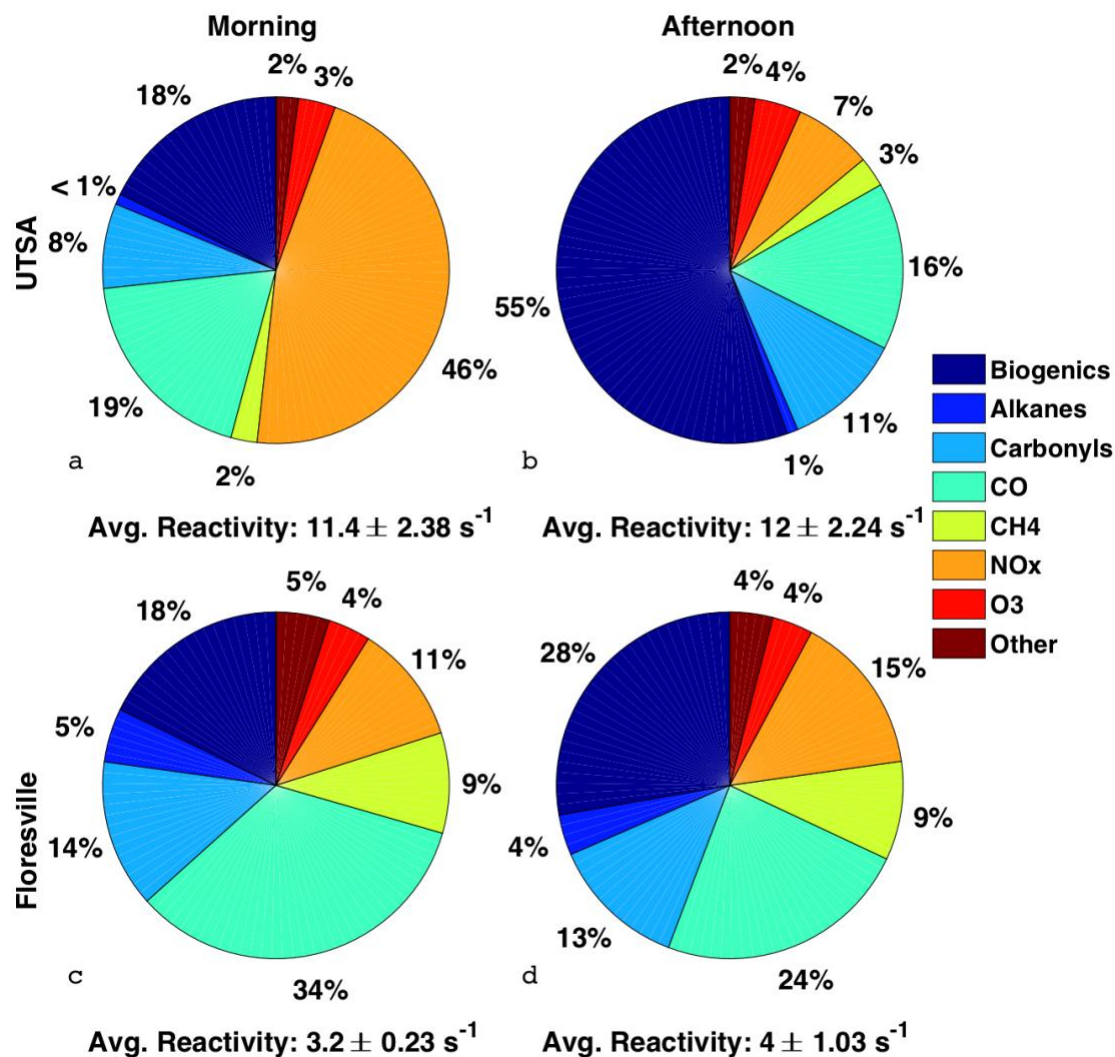
Figure 8: The distribution of the various contributors to the overall OH reactivity for the UTSA (13 -16 May) and Floresville (17 – 19 May) sites are shown for both the morning, times between 7:00 and 11:00, and afternoon, times between 13:00 and 20:00. The average OH reactivity ($\pm 1\sigma$) is also shown.

873
874
875